Research paper

Three new Ag(I) thiosaccharinate complexes: Synthesis, structural studies, spectral characterization and theoretical analysis

Robert A. Burrow [a,*], Giancarlo Z. Belmonte [a], Viviana Dorn [b], Mariana Dennehy [b,*]

[a] Laboratório de Materiais Inorgânicos, Departamento de Química, Universidade Federal de Santa Maria, 97105-900 Santa Maria, RS, Brazil
[b] INQUISUR-Departamento de Química, Universidad Nacional del Sur, Avda. Alem 1253, B8000CPB Bahía Blanca, Argentina

ABSTRACT

Three silver thiosaccharinate complexes, two of them with diverse coordination geometries controlled by the ancillary nitrogen donor ligands are presented. The dinuclear silver thiosaccharinate complex, *catena*-poly-[Ag$_2$(tsac)$_2$]·C$_3$H$_7$NO (**1·DMF**), (thiosaccharinate = thiosaccharinate anion, DMF = dimethylformamide) in the crystalline state is a one dimensional coordination polymer bridged by the thiosaccharinate ligand with a very short silver–silver distance, 2.8930(16) Å. The biquinoline silver(I) thiosaccharinate, [Ag(tsac)(2,2′-bquin)]·CH$_3$CN (**2·CH₃CN**), (bquin = 2,2′-biquinoline) in the crystalline state consists of a mononuclear neutral unit solvated with an acetonitrile molecule. The double complex salt, [Ag(2,4,6-coll)$_2$][Ag(tsac)$_2$] (**3**), (2,4,6-coll = 2,4,6-collidine) possesses a very unusual arrangement for a silver thiosaccharinate, one similar to an ionic silver-pyridine based structure. The complex cation is formed by two 2,4,6-trimethylpyridine molecules coordinated to the silver atom while the complex anion is composed of two thiosaccharinate anions coordinated to the silver atom. In both cation and anion, the silver center has a linear geometry with the ligands planar. The syntheses, full characterizations and crystal structures of the three complexes are described. The structures of these newly synthesized silver(I) thiosaccharinate complexes have been optimized and their structural parameters have been calculated at the B3LYP/6-31G(2d,p)/LANL2DZ level of theory. The ^{13}C NMR chemical shifts for the DMSO solution species of (**2**) and (**3**) were calculated using DFT/EPR-III/DZP first principles calculations with B3LYP, OLYP, OPBE, HCTH93 functionals.

© 2016 Elsevier B.V. All rights reserved.

1. Introduction

Thiosaccharine, 1,2-benzoisothiazol-3-(2H)-thione-1,1-dioxide, is the precursor to the electron-rich and poly-functional thiosaccharinate anionic ligand (Scheme 1). In the figure of the thiosaccharinate anion, the red area of the electrostatic potential mapped to the isoelectron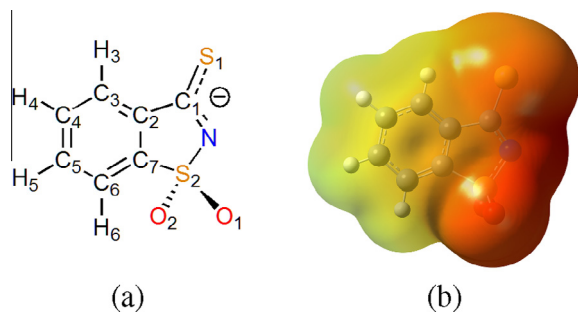ic density surface shows the negative charge dispersed over the soft sulfur atom and the hard nitrogen atom. The ambidentate nature of the ligand allows it to coordinate to either soft or hard metal centers. The close proximity of the two possible coordinating atoms permits a variety of bridging coordination modes as detailed below, and can produce anywhere from mononuclear to complex polynuclear species [1]. Systematic studies of thiosaccharinate metal complexes have produced complexes with Cd(II) [2–4], Tl(I) [5], Pb(II) [6], Ag(I) [7–12], Cu(I) [13–15], Pd(II) [16], Au(I) [17], Bi(III) [18,19] and recently Pt(II) [20–22]. Silver (I) coordination complexes containing N or S donor atom ligands present particular interest because their known antibacterial effects [23,24].

The versatility of the thiosaccharinate anion is highlighted further in silver thiosaccharinate complexes with ancillary ligands in which the thiosaccharinate ligand usually binds in a μ$_2$-S,N coordination mode with either a head-to-head or a head-to-tail arrangement [25]. The variety of the binding modes of the thiosaccharinate ligand is seen for the binary silver thiosaccharinate complex which has been crystallized as two different

Scheme 1. Thiosaccharinate anion, with usual numbering scheme (a) and the molecular structure overlaid with the electrostatic potential mapped on an isoelectronic surface with red negative and green positive, calculated at the B3LYP/6-31G**//B3LYP/6-311G** levels (b). (For interpretation of the references to color in this figure legend, the reader is referred to the web version of this article.)

complexes—the hexameric $[Ag_6(tsac)_6]$ [1] and the one dimensional extended structure $[Ag(tsac)]_n$ [7]—depending on the synthetic pathway. The thiosaccharinate ligands shows diverse bonding modes—such as S-monocoordinated; S,N-head to tail; S-bridge; S,N-head to head—in ternary Ag(tsac) complexes with pyridine based ancillary ligands [7–12].

We present here new contributions to silver thiosaccharinate crystal chemistry. A new form of the one-dimensional extended silver thiosaccharinate is obtained by recrystallization of the hexameric $[Ag_6(tsac)_6]$ in dimethylformamide, catena-poly-$[Ag_2(tsac)_2]_n$·DMF (**1·DMF**), with DMF as solvate in the crystalline state. The syntheses of new silver thiosaccharinates with two sterically hindered N-donor co-ligands—the monodentate 2,4,6-collidine (2,4,6-coll) and the bidentate 2,2′-biquinoline (2,2′-bquin)—were undertaken to understand the behavior of the tertiary Ag thiosaccharinate N donor systems. These give the double complex salt $[Ag(2,4,6-coll)_2][Ag(tsac)_2]$ (**2**)—the first ionic silver thiosaccharinate complex–and $[Ag(tsac)(2,2′-bquin)]·CH_3CN$ (**3·CH₃CN**), respectively. The crystal structures and full spectroscopic characterizations of these three new compounds are detailed. A comparison of the thiosaccharinate bonding modes is presented.

Further insight into the molecular structure of the complexes was provided by theoretical calculations using the DFT approach. Firstly, gas-phase optimization starting from coordinates derived from the single crystal structure was performed, which gave a similar structure and was used to confirm the vibrational spectra. Secondly, a solvent phase optimization to simulate the ^{13}C NMR was performed using a selection of DFT functionals—B3LYP, B97-2, B98, OLYP, OPBE and HCTH93—with OLYP and HCTH93 functionals producing very good results for the magnetic shielding values.

2. Experimental

2.1. General remarks

All chemicals were of analytical reagent grade and used as purchased. Solid thiosaccharin (Hthiosaccharinate) in its α-form was prepared by the reaction of saccharin (3.00 g; Mallinckrodt) with Lawesson's reagent (3.64 g; Fluka) in toluene (25 mL), following the technique published by Schibye et al. [26], and characterized by melting point and infrared (IR) spectroscopy analysis. The $[Ag_6(tsac)_6]$ complex was synthesized as previously reported [1].

The IR spectra of the substances as KBr pellets were recorded in the 4000–400 cm^{-1} range on a Nicolet Nexus FTIR spectrometer. Nuclear magnetic resonance (NMR) spectra were recorded on a Bruker ARX-300 spectrophotometer using the residual solvent peak as an internal reference. Experiments were performed in

deuterated dimethylsulfoxide, DMSO-d_6. The C, H, and N elemental analyses were performed with a Thermo ElectronFlashEA 1112 Elemental Analyzer. The nitrogen adsorption analysis was carried out on a Quantachrome NOVA 1200e at 77 K.

The geometries of complexes (**2**) and (**3**) were optimized by means of density functional theory (DFT) quantum-mechanical calculations [27] using the gradient corrected Becke's three parameters hybrid exchange function in combination with the correlation function of Lee, Yang and Parr (B3LYP) [28–31] as implemented in the software package GAUSSIAN09 [32]. Geometry optimization procedures were started from the experimental crystallographic data of $[Ag(tsac)(2,2′-bquin)]$ and $[Ag(2,4,6-coll)_2][Ag(tsac)_2]$ employing the LANL2DZ effective core potential basis set for Ag atoms and the 6-31G(2d,p) basis sets for the C, H, S, N and O atoms without symmetry constraints, using the 'tight' optimization criteria and 'ultrafine' integration grids. The resulting geometry was confirmed to be at a potential energy minimum by vibrational frequency analysis (no imaginary frequencies). The NMR solution phase chemical shifts for (**2**) and (**3**) were determined using the energy minimized structures of each species, considering the cation and the anion of (**3**) separately, in dimethylsulfoxide (DMSO) using the integral equation formalism model (IEFPCM) [33] in GAUSSIAN09 with the built in parameters for this solvent, and the B3LYP hybrid DFT functional with the LanL2DZ ECP basis set for Ag and 6-31(2d,p) basis sets for the other elements using the 'tight' optimization criteria and 'ultrafine' integration grids. The NMR magnetic shielding calculations were performed with the hybrid density functionals B3LYP, B97-2 [34] and B98 [35] with the Gauge-Including Atomic Orbitals (GIAO) method [36] and the newer generalized gradient approximation (GGA) density functionals HCTH93 [37], OPBE [38] and OLYP—the last two based on Handy's OptX exchange functional [38,39]—with the Continuous Set of Gauge Transformations (CSGT) method [40], all with the DZP all core basis set [41] for Ag atoms, EPR-III basis sets for H, C, N and O atoms, and aug-cc-pvdz for S atoms and 'ultrafine' integration grids. The DZP basis set was obtained from the EMSL Basis Set Library [42,43].

2.2. Crystallography

Single crystal X-ray diffractions studies were performed on a Bruker X8 Kappa APEX II CCD single crystal diffractometer equipped with a Mo anode fine long focus sealed ceramic tube operating at 50 kV and 35 mA, and planar graphite monochromator. The crystals were glued to fine glass fibers. For the low temperature study, a Bruker Kryoflex low temperature unit was used. Data Collection: Bruker APEX2/BIS/COSMO; cell refinement: Bruker SAINT; data reduction: Bruker SAINT/SADABS [44]. Programs used to solve and refine structure: Bruker XT and XL (Bruker SHELXTL) [45]; molecular graphics: Crystal Impact Diamond 3 (version 3.2k) [46] and Mercury CSD (version 3.6 RC6) [47].

For (**1·DMF**), SQUEEZE [PLATON version 01/10/2015] [48] was used to remove 157 electrons from the unit cell for highly disordered solvent found in columns running in the [0 0 1] crystallographic direction with a total volume of 418 Å³. This value corresponds to roughly four dimethylformamide solvate molecules (40 electrons each) per unit cell. The proposed molecular formula, $[Ag_2(C_7H_4NO_2S)_2]·C_3H_7NO$, was used to generate the absorption coefficient, crystal density and F_{000} values. Details of the single crystal X-ray experiments and crystal data are summarized in Table 1.

The powder X-ray diffraction experiment was performed on a Philips W 1710 equipped with a Cu anode sealed X-ray tube operating at 45 kV and 30 mA. The data collection was made on packed samples with Bragg–Brentano geometry in θ–θ mode.

Table 1
Crystal data and structure refinements for (**1·DMF**), (**2**) and (**3·CH₃CN**).

	(**1·DMF**)	(**2**)	(**3·CH₃CN**)
Empirical formula	$C_{14}H_8Ag_2N_2O_4S_4 \cdot C_3H_7NO$	$C_{30}H_{30}Ag_2N_4O_4S_4$	$C_{25}H_{16}AgN_3O_2S_2 \cdot CH_3CN$
Formula weight	685.30	854.56	603.45
T (K)	296(2)	296(2)	100(2)
λ (Å)	0.71073	0.71073	0.71073
Crystal system	monoclinic	orthorhombic	monoclinic
Space group	$C2/c$	$Pbam$	$P2_1/c$
Unit cell dimensions			
a (Å)	18.7548(15)	8.2387(6)	14.297(7)
b (Å)	13.2954(10)	27.843(2)	22.252(13)
c (Å)	8.2349(6)	6.9844(6)	7.449(3)
β (°)	94.198(3)		102.679(16)
V (Å³)	2047.9(3)	1602.2(2)	2312(2)
Z	4	2	4
D_{Calc} (Mg m⁻³)	2.223	1.771	1.734
Absorption coefficient (mm⁻¹)	2.358	1.525	1.088
$F(000)$	1344	856	1216
Crystal size (mm)	$0.77 \times 0.04 \times 0.02$	$0.48 \times 0.08 \times 0.05$	$0.51 \times 0.05 \times 0.02$
θ range for data collection (°)	3.61–27.11	3.83–30.53	3.92–28.33
Index ranges	$-24 \leqslant h \leqslant 24$,	$-11 \leqslant h \leqslant 11$,	$-19 \leqslant h \leqslant 16$,
	$-17 \leqslant k \leqslant 16$,	$-39 \leqslant k \leqslant 39$,	$-27 \leqslant k \leqslant 29$,
	$-8 \leqslant l \leqslant 10$	$-9 \leqslant l \leqslant 9$	$-8 \leqslant l \leqslant 9$
Reflections collected	9552	24584	16041
Independent reflections	2211 [$R_{int} = 0.0489$]	2618 [$R_{int} = 0.0790$]	5678 [$R_{int} = 0.1211$]
Completeness	97.5% [$\theta = 27.11°$]	99.5% [$\theta = 30.53°$]	98.6% [$\theta = 28.33°$]
Absorption correction	numerical	numerical	numerical
Maximum and minimum transmission	0.9875 and 0.8609	1.0000 and 0.7232	1.0000 and 0.8335
Data/restraints/parameters	2211/0/118	2618/0/134	5678/0/326
Goodness-of-fit (GOF) on F^2	1.143	0.979	0.976
Final R indices [$I > 2\sigma(I)$]	$R_1 = 0.0557$,	$R_1 = 0.0536$,	$R_1 = 0.0709$,
	$wR_2 = 0.1001$	$wR_2 = 0.1323$	$wR_2 = 0.1231$
R indices (all data)	$R_1 = 0.0918$,	$R_1 = 0.1349$,	$R_1 = 0.1513$,
	$wR_2 = 0.1095$	$wR_2 = 0.1684$	$wR_2 = 0.1621$
Largest difference peak and hole (e Å⁻³)	0.591 and −0.834	1.064 and −1.186	0.890 and −1.513

2.3. Synthesis

2.3.1. catena-Poly-[Ag₂(tsac)₂]ₙ·½C₃H₇NO (**1·½DMF**)

The [Ag₂(tsac)₂]·½C₃H₇NO complex was prepared by dissolution of 0.010 g of [Ag₆(tsac)₆] in 5 mL of dimethylformamide (DMF). A clear yellow solution was obtained. By slow diffusion of diethyl ether very thin yellow needles were produced. Yield: 86% Analytical percent composition calculated for C₁₄H₈Ag₂N₂O₄S₄·½C₃H₇NO: C, 28.70; H, 1.79; N, 5.40. Found: C, 28.86; H, 1.74; N, 5.48%.

Selected anion bands for [Ag₂(tsac)₂]·½C₃H₇NO, KBr: (cm⁻¹). ν (NC),ν(CS),δ_{PhH}, ν (CC), 1409m; ν_{as}(SO₂), 1316s; ν_{as}(ϕCN),δ(CH), 1239m; ν_s(SO₂),ν(CC), 1171s; ν_s(SO₂),δ(ϕSN), 1122w; ν(CS),δ(CNS), 1012m; ν(NS),δ(CCC), 806w; γ(SO₂),δ(ϕCN), 624w.

2.3.2. [Ag(2,4,6-coll)₂][Ag(tsac)₂] (**2**)

The [Ag(2,4,6-coll)₂][Ag(tsac)₂] was prepared by reaction of [Ag₆(tsac)₆] (8 mg, 0.026 mmol) in 3 mL of collidine. Slow diffusion of diethylether into a saturated solution of this compound yielded yellow crystals. Yield: 63%. Analytical percent composition calculated for C₁₅H₁₅AgN₂O₂S₂: C, 42.17; H, 3.54; and N, 6.56. Found: C, 41.81; H, 3.53; and N, 6.80%.

Selected anion bands for [Ag(2,4,6-coll)₂][Ag(tsac)₂], KBr: (cm⁻¹). ν(NC),ν(CS), δ_{PhH}, ν (CC), 1422w; ν_{as}(SO₂), 1310s; ν_{as}(ϕCN),δ(CH), 1234s; ν_s(SO₂),ν(CC), 1164vs; ν_s(SO₂), δ(ϕSN), 1124w; ν(CS),δ(CNS), 999m; ν(NS),δ(CCC), 792m; γ(SO₂), δ(ϕCN).

¹H NMR (300 MHz, DMSO) δ 7.99–8.08 (m, 2H), 7.86–7.95 (m, 2H), 7.75–7.83 (m, 4H), 6.96 (s, 4H), 2.44 (s, 12H), 2.25 (s, 6H). ¹³C NMR (75 MHz, DMSO) δ 187.35 (C1), 156.49 (C8), 148.72 (C11), 137.79 (C7), 133.95 (C2), 133.57 (C5), 132.74 (C4), 125.41 (C3), 121.58 (C10), 120.37 (C6), 23.90 (C9), 20.35 (C12).

2.3.3. [Ag(tsac)(2,2′-bquin)]·CH₃CN (**3·CH₃CN**)

The [Ag(tsac)(2,2′-bquin)]·CH₃CN complex was obtained by the addition of solid [Ag₆(tsac)₆] (10 mg, 0.032 mmol) to a solution of 2,2′-biquinoline (8.36 mg, 0.032 mmol) in CH₃CN. After 12 days of slow diffusion of CH₂Cl₂ into a saturated solution very thin needles crystals suitable for X-ray diffraction studies were obtained. Yield: 44%. Analytical percent composition calculated for C₂₅H₁₆-AgN₃O₂S₂; C, 53.39; H, 2.87; N 7.47. Found: C, 52.83; H, 2.88; N, 8.04%.

Selected anion bands for [Ag(tsac)(2,2′-bquin)]·CH₃CN, KBr: (cm⁻¹). ν(NC), ν(CS), δ_{PhH}, ν(CC), 1410m; ν_{as}(SO₂), 1309s; ν_{as}(ϕ CN),δ(CH), 1227m; ν_s(SO₂),ν(CC), 1163s; ν_s(SO₂), δ(ϕSN), 1121w; ν(CS),δ(CNS), 1000m; ν(NS),δ(CCC), 807w; γ(SO₂), δ(ϕCN), 626w.

¹H NMR (300 MHz, DMSO) δ 8.76 (q, $J = 8.6$ Hz, 2H), 8.51 (d, $J = 8.6$ Hz, 1H), 8.13 (d, $J = 7.7$ Hz, 1H), 8.04–8.08 (m, 1H), 7.85–7.95 (m, 2H), 7.77–7.82 (m, 2H), 7.74 (t, $J = 7.7$, 1H). ¹³C NMR (75 MHz, DMSO) δ 187.43 (C1), 152.97 (C8), 146.38 (C12), 138.92 (C10), 138.11 (C7), 134.23 (C2), 133.49 (C15), 132.55 (C4), 131.05 (C5), 130.10 (C16), 128.55 (C11), 128.12 (C13), 128.01 (C14), 125.23 (C3), 120.32 (C9), 119.79 (C6).

3. Results and discussion

3.1. Syntheses

3.1.1. catena-[Ag₂(tsac)₂]·DMF (**1·DMF**)

The syntheses of the complexes reported here all used [Ag₆(tsac)₆] as starting material. The hexanuclear complex in coordinating solvents is broken down likely to a dinuclear species [Ag₂(tsac)₂]—however, a monomeric [Ag(tsac)] species cannot be ruled out—either one presumably suitably solvated. When

$[Ag_6(tsac)_6]$ is crystallized from acetonitrile, the hexameric complex is formed [1], whereas from dimethylsulfoxide, the two dimensional coordination polymer *phyllo*-poly-$[Ag_2(tsac)_2]$ is formed in the solid state, without presence of the solvent in the crystal [7]. In the first, a set of three pairs of {Ag(tsac)} units closes to form a trigonal antiprism of silver atoms and, in the second, a two-dimensional extended structure is formed. In this work, from dimethylformide, DMF, $[Ag_6(tsac)_6]$ is crystallized as the one-dimensional *catena*-poly-$[Ag_2(tsac)_2]$ (**1**) with the solvent filling 8 Å channels. In all three complexes, the thiosaccharinate ligand binds via the nitrogen atom to one just silver atom and bridges with the sulfide atom across two other silver atoms with neighboring thiosaccharinate ligands binding in a head-to-tail fashion, Scheme 2.

The single crystal X-ray structural determination of (**1**) finds one DMF solvate molecule per $Ag_2(tsac)_2$ unit, giving the formula (**1·DMF**). The elemental analysis, repeated on three different samples, of the as-synthesized (**1**) gave results consistent with half a DMF solvate molecule per $Ag_2(tsac)_2$ unit, resulting in a putative formula (**1·½DMF**). The powder X-ray diffractogram of freshly prepared (**1·½DMF**) is very similar to that simulated from the crystal cell and atomic data of the single crystal X-ray experiment of (**1·DMF**), Fig. S2 in Supplementary material. The close positions of the diffraction peaks suggest an identical cell, while the difference in peak areas could be due to a range of packing and diffraction effects in the powder X-ray diffraction experiment in addition to any small deviations due to differences in quantity of solvated DMF.

3.1.2. [Ag(2,4,6-coll)₂][Ag(tsac)₂] (2)

Complex (**2**), $[Ag(2,4,6-coll)_2][Ag(tsac)_2]$, is the first thiosaccharine argentate reported to date, consisting of the bis(2,4,6-collidine)silver(+1) cation and bis(thiosaccharinato)silver(−1) anion in the crystalline state. Silver salts of non-coordinating anions dissolved in water or in other coordinating solvents (DMSO, MeCN, DMF), in the presence of an excess amount of pyridine or other pyridine based, present the $[AgL_2]^+$ cations as the dominant species (L = pyridine based) [49,50]. In the case of solutions in pure pyridine, the principal species has been determined to be the $[AgL_4]^+$ cation. Crystalline $[AgL_2]X$ or $[AgL_4]X$ solids (X = non-coordinating anion) are commonly recovered, respectively, from these solutions. When $[Ag_6(tsac)_6]$ was dissolved in pure or concentrated solutions of pyridine and other pyridine based, $[AgL_2]^+$ or $[AgL_4]^+$ species have been never recovered until now. Dinuclear or polynuclear silver–thionato–pyridine based complexes were always formed as insoluble or sparingly soluble covalent solids. When $[Ag_6(tsac)_6]$ was dissolved in 2,4,6-collidine, the obtained complex was surprisingly the double complex ionic species $[Ag(2,4,6-coll)_2][Ag(tsac)_2]$. It is surmised that the *ortho*-methyl groups, though not large, are

sufficiently large enough to block the thiosaccharinate from also coordinating the same silver center but do not interfere with one another in the near planar $[Ag(2,4,6-coll)_2]^+$ cation.

### 3.1.3. [Ag(tsac)(2,2′-bquin)]·CH₃CN (3·CH₃CN)

From $[Ag_6(tsac)_6]$ and 2,2′-biquiniline in acetonitrile, the complex $[Ag(tsac)(2,2′-bquin)]·CH_3CN$ (**3·CH₃CN**) is formed. A detailed discussion of the thiosaccharinate coordination to the silver center is presented below.

3.2. Crystal structures

3.2.1. catena-Poly-[Ag₂(tsac)₂]ₙ·C₃H₇NO (1·DMF)

The crystal structure of (**1·DMF**) shows an extended one-dimensional structure in the crystallographic *z* direction made of $[Ag_2(tsac)_2]$ units joined by double S bridges in which the thiosaccharinate ligands bond to three silver atoms in a μ_3-S,N manner (μ_2-S and μ-N) (Fig. 2). In each $[Ag_2(tsac)_2]$ unit, the thiosaccharinate ligands bridge the two Ag atoms with the endocyclic nitrogen atoms and with the exocyclic sulfur atoms in a head-to-tail planar fashion, across a crystallographic inversion center midway between the Ag atoms, to form the dinuclear centrosymmetric unit. The thiosaccharinate ligands also form a slightly longer bond with the S atom to another Ag atom to create the double S bridges. The linear extended structures pack loosely together in the unit cell leaving large channels which are lined on two opposite sides by O atoms and Ag atoms while phenyl groups line the other two, giving the channel both hydrophilic and hydrophobic character, Fig. 3. The electron density corresponding to the atoms of the DMF molecules was not localized. Using the SQUEEZE routine within PLATON [48], density electronic summing to 157 electrons per unit cell was removed from the unit cell and the reflection intensities corrected to account for the removal. The number of electrons corresponds well to four DMF molecules per unit cell. In the crystalline state, per unit cell there are four formula units $[Ag_2(tsac)_2]$ of (**1·DMF**). This gives a stoichiometric ratio of $[Ag_2(tsac)_2]·DMF$ for the crystal measured. As noted above, the as-synthesized compound consistently gives an elemental analysis consistent with the hemisolvate, $[Ag_2(tsac)_2]·½C_3H_7NO$ (**1·½DMF**). We presume with handling, the fresh DMF solvated crystals gradual lose solvent, giving an average of half the solvent at time of analysis. With the removal of the DMF molecules, there remains a total void volume is 20.4% (418 Å³). A gas adsorption analysis of the desolvated powder shows a Type IV adsorption curve with Type H3 hysteresis [51], Fig. 1. This is consistent with a mesoporous capillary network [52]. A *t*-Plot analysis [53] of the isotherm shows no microporosity, expected with the 8 Å diameter channels seen in the crystal structure of (**1**), which could be due to incomplete capillary desolvation or other capillary blockage.


(a)   (b)   (c)
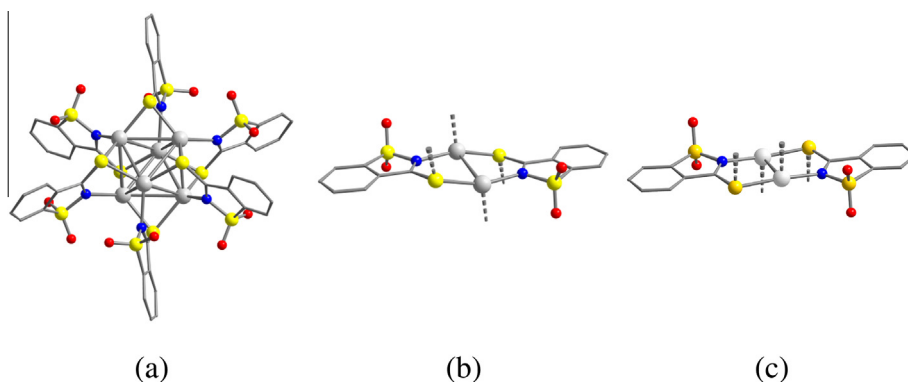
Scheme 2. Binary Ag(tsac) complexes: $[Ag_6(tsac)_6]$ [1] (a), *phyllo*-$[Ag_2(tsac)_2]_n$ [7] (b) and *catena*-$[Ag_2(tsac)_2]$ [this work].
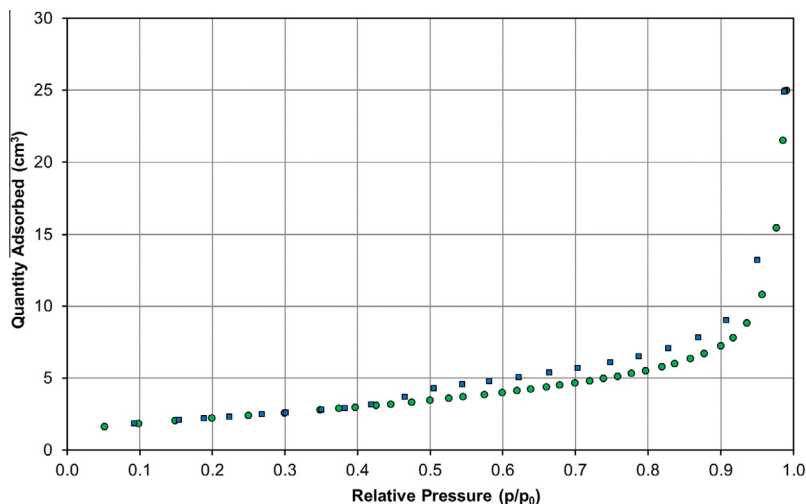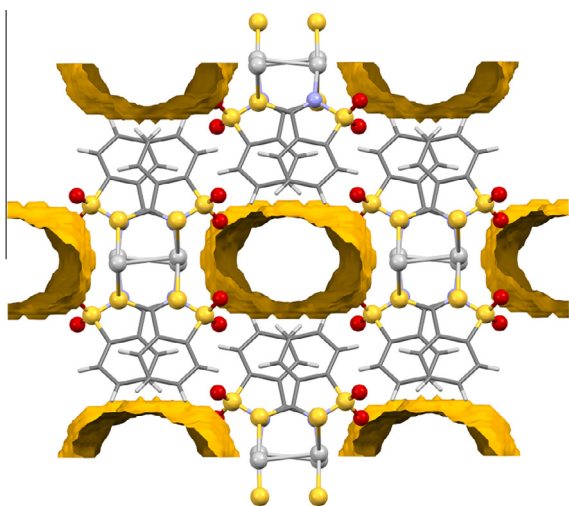
Fig. 1. Adsorption/desorption isotherm of N2 at 77 K on (**1**); the green filled circles are the adsorption part and the blue filled squares are the desorption part of the isotherm. (For interpretation of the references to color in this figure legend, the reader is referred to the web version of this article.)
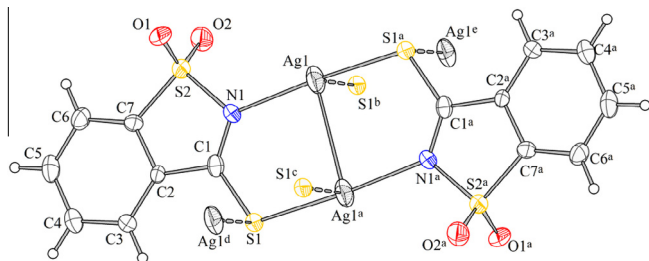
Fig. 2. Molecular structure of (**1**), *catena*-poly-[Ag$_2$(tsac)$_2$]$_n$. Thermal displacement representation with 30% ellipsoids, showing atomic numbering scheme. Symmetry operators: [a] 1 − x, 1 − y, 1 − z; [b] x, 1 − y, −½ + z; [c] 1 − x, y, ³/₂ − z; [d] x, 1 − y, ½ − z; [e] 1 − x, y, ½ − z.
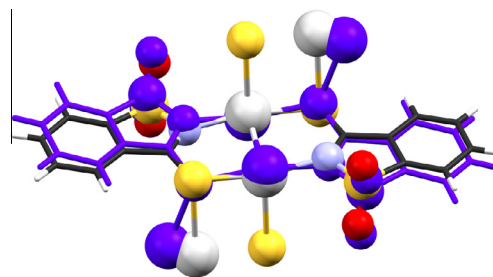
Fig. 4. Overlay of the core of (**1**), with that of *phyllo*-[Ag$_2$(tsac)$_2$]$_n$, in blue, from Ref. [7]. (For interpretation of the references to color in this figure legend, the reader is referred to the web version of this article.)

Table 2
Selected bond distances and angles [Å, °] for the two dimers [Ag$_2$(tsac)$_2$]$_n$.

phyllo-[Ag$_2$(tsac)$_2$]$_n$ (Ref. [7])		(1) *catena*-Poly-[Ag$_2$(tsac)$_2$]$_n$·DMF (this work)	
Ag(1)–N(1)	2.199(2)	Ag(1)–N(1)	2.174(5)
Ag(1)–S(1)	2.4111(7)	Ag(1)–S(1)[a]	2.3996(17)
Ag(1)–S(1)	2.8031(7)	Ag(1)–S(1)[b]	3.041(2)
Ag(1)···Ag(1)	2.9194(4)	Ag(1)···Ag(1)[a]	2.8893(17)
C(1)–N(1)	1.320(3)	C(1)–N(1)	1.307(9)
C(1)–S(1)	1.704(2)	C(1)–S(1)	1.683(7)
N(1)–Ag(1)–S(1)	161.93(6)	N(1)–Ag(1)–S(1)[a]	169.92(17)
N(1)–Ag(1)–S(1)	90.60(6)	N(1)–Ag(1)–S(1)[b]	95.81(16)
S(1)–Ag(1)–S(1)	107.45(2)	S(1)[a]–Ag(1)–S(1)[b]	92.89(6)
N(1)–Ag(1)–Ag(1)	87.89(6)	N(1)–Ag(1)–Ag(1)[a]	85.88(16)
S(1)–Ag(1)–Ag(1)	84.458(18)	S(1)[a]–Ag(1)–Ag(1)[a]	87.82(6)
S(1)–Ag(1)–Ag(1)	112.273(19)		

Symmetry elements:
[a] 1 − x, 1 − y, 1 − z.
[b] x, 1 − y, −½ + z.

Fig. 3. The solvent contact surfaces, outlined in brown, in the crystal structure of (**1**), viewing along the crystallographic *c* axis into page, with the *a* axis down and the *b* axis to the left. (For interpretation of the references to color in this figure legend, the reader is referred to the web version of this article.)

The overall structure of (**1·DMF**) is very different from the crystal structure of *phyllo*-[Ag$_2$(tsac)$_2$]$_n$ complex reported previously by our group [7], which is a two dimensional extended structure. The [Ag$_2$(tsac)$_2$] unit in the *phyllo* structure is very similar to that in the *catena* structure, featuring a near planar geometry with the thiosaccharinate ligands bridging between the two Ag atoms with N and S atoms in a head-to-tail planar fashion in both units, Fig. 4. A comparison between bond distances and angles of the two dimers [Ag$_2$(tsac)$_2$]$_n$ can be found in Table 2. The Ag–N$_{endo}$ bond distance, 2.174(5) Å is shorter than the Ag–N$_{endo}$ in [Ag$_6$(tsac)$_6$] (2.285(2) Å). The tendency of silver(I) ions to aggregate themselves, reported as "argentophilicity", contributes to the stabilization of the molecular structures. The Ag–Ag distance, 2.8893 (17) Å, is shorter in this complex than that in the previously
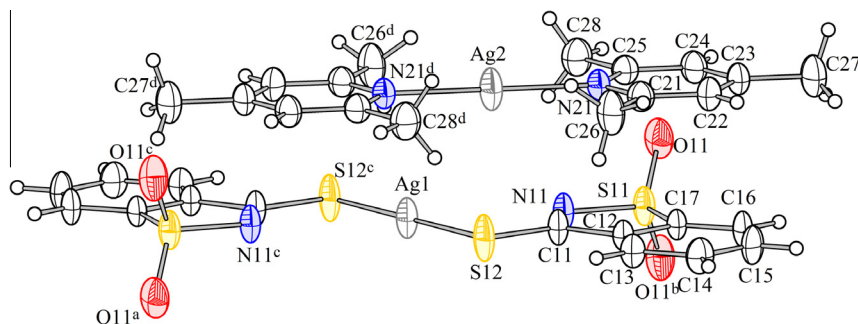
Fig. 5. Molecular structure of the [Ag(2,4,6-coll)₂][Ag(tsac)₂] (**2**) complex with atomic numbering scheme drawn with thermal ellipsoids at the 30% probability level. Symmetry operators: ᵃ −x, −y, −z; ᵇ x, y, −z; ᶜ −x, −y, z; ᵈ 1 − x, −y, 1 − z.

Table 3
Selected bond distances and angles [Å, °] for [Ag(2,4,6-coll)₂][Ag(tsac)₂] (**2**).

	Experimental (crystal structure)	Calculated (gas phase DFT)
Anion		
Ag(1)–S(12)	2.3532(17)	2.459
S(12)–C(11)	1.698(6)	1.719
C(11)–N(11)	1.315(7)	1.309
S(12)–Ag(1)–S(12)ᵃ	180	180
Ag(1)–S(12)–C(11)	100.5(2)	101.0
S(12)–C(11)–N(11)	124.6(4)	125.0
Cation		
Ag(2)–N(21)	2.148(5)	2.174
N(21)–C(21)	1.338(8)	1.353

Symmetry element: ᵃ −x, −y, −z.

Table 4
Selected bond distances and angles [Å, °] for [Ag(tsac)(2,2′-biquin)]·CH₃CN (**3**).

	Experimental (Crystal structure)	Calculated (gas phase DFT)
Ag(1)–S(1)	2.393(2)	2.472
Ag(1)–N(11)	2.327(5)	2.398
Ag(1)–N(21)	2.290(7)	2.431
C(1)–S(1)	1.709(7)	1.727
C(1)–N(1)	1.304(9)	1.311
N(21)–Ag(1)–N(11)	71.5(2)	69.817
N(21)–Ag(1)–S(1)	154.02(14)	151.965
N(11)–Ag(1)–S(1)	134.25(16)	136.85
N(1)–C(1)–C(2)	116.2(6)	115.4
N(1)–C(1)–S(1)	124.7(5)	123.98

Fig. 6. Molecular structure of the [Ag(tsac)(2,2′-biquin)]·CH₃CN complex, (**3**), showing numbering scheme with thermal displacement ellipsoids at the 50% probability level.

reported *phyllo* structure and can be considered as strong argentophilic interaction according to the criteria presented by different authors, as Kristiansson and Chen et al. [50,54,55]. In (**1**), the Ag–S$_{exo}$ bond distance in the dimeric unit is 2.3996(17) Å, shorter than the distances observed for [Ag₆(tsac)₆] (2.4860(7) and 5.5012(7) Å). The C–S$_{exo}$ bond distance also reflects the change in the strength of the coordination of the S$_{exo}$ to the metal atom of the dimer versus the coordination in [Ag₆(tsac)₆]. A single bridging
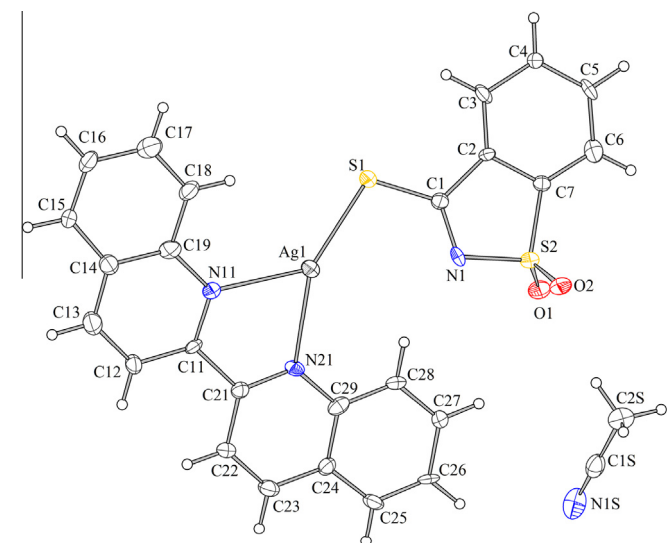
atom (S$_{exo}$) is linking successive silver atoms. The distance of this long Ag–S$_{exo}$ interaction, 3.041(2) Å, is longer than the sum of the covalent atom radii, considered in the 2.43–2.60 Å [56], but less than the sum of the van der Waals radii (3.52 Å) [57].

3.2.2. [Ag(2,4,6-coll)₂][Ag(tsac)₂] (*2*)

Both the anion and cation of the double complex salt [Ag(2,4,6-coll)₂][Ag(tsac)₂] (**2**) are situated on crystallographic mirror planes, giving ions with planar geometries, and in both, the silver center is two coordinate with approximately linear geometry. The complex cation shows a classical arrangement for the bis(2,4,6-trimethyl-pyridine)silver(I) ion, Fig. 5. Bowmaker and coworkers [58] have presented some [AgL₂]X structures (X being a non-coordinating anion). Within the 2,4,6-trimethylpyridine moieties, the bond distances and angles are in the order of those previously reported by Bond and Davies for the pure ligand [59] (C—N 1.345 and 1.347 Å versus 1.338(8) and 1.352(8) Å for (**2**). Compared to N$_{Py}$–Ag bond distance in [Ag₂(tsac)₂Py] [10] (2.352 Å) N$_{coll}$—Ag bond distance is shorter (2.148(5) Å). Within the five membered ring of the [Ag(tsac)₂] anion, the Ag–S$_{exo}$, C11—S$_{exo}$ and the N$_{endo}$—C11 bond distances—2.3535(17), 1.698(6) and 1.315(7) Å, respectively—are very similar to those presented in (**3**), see below, corresponding to a monocoordinated sulfur anion. Selected bond lengths and angles for (**2**), along with gas phase calculated values (see below), are presented in Table 3.

3.2.3. [Ag(tsac)(2,2′-bquin)]·CH₃CN (*3·CH₃CN*)
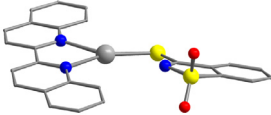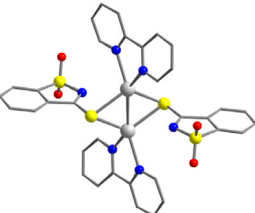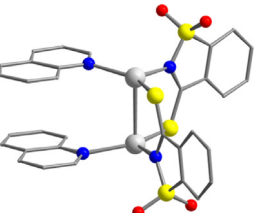
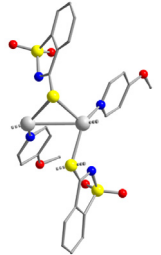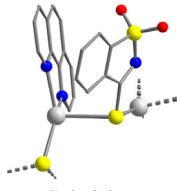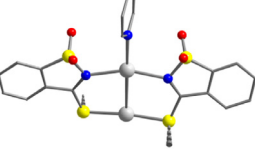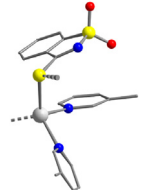The ternary 2,2′-biquinoline thiosaccharinate silver complex [Ag(tsac)(bquin)]·CH₃CN, **3**, consists of neutral mononuclear units with acetonitrile molecule as solvate in its crystalline form. The free 2,2′-biquinoline molecule in crystalline form presents a *trans* conformation, however when coordinated to metal centers it is always found in the *cis* form [60–62]. The monomeric unit of **3** is presented in Fig. 6. In a first approximation the silver coordination

Table 5
Comparison of the thiosaccharinate ligand bonding modes in ternary Ag(tsac)(L) complexes.

	Compound, nuclearity	pK_a[a]	Molar ratio[b]	Structure anion coordination	Ref.
1	[Ag(tsac)(2,2′-biquinoline)], mononuclear	2.82	1:1:1	 S-monocoordinated	[This work]
2	[Ag$_2$(tsac)$_2$(2,2′-bipyridine)$_2$], dinuclear	4.33	1:1:1	 S-monocoordinated	[8]
3	[Ag$_2$(tsac)$_2$(quinoline)$_2$], dinuclear	4.90	1:1:1	 S, N-head to tail	[11]
4	catena-Poly-[Ag(tsac)(4-methoxylpyridine)$_2$]$_n$, polymeric	4.78	1:1:1	 S-bridge	[12]
5	catena-Poly-[Ag(tsac)(o-phenanthroline)]$_n$, polymeric	4.84	1:1:1	 S-bridge	[9]
6	catena-Poly-[Ag$_2$(tsac)$_2$(pyridine)]$_n$, dinuclear	5.23	2:2:1	 S, N-head to head	[10]
7	catena-Poly-[Ag(tsac)(3-methylpyridine)$_2$]$_n$, polymeric	5.70	1:1:2	 S-bridge	[12]

Table 5 (continued)

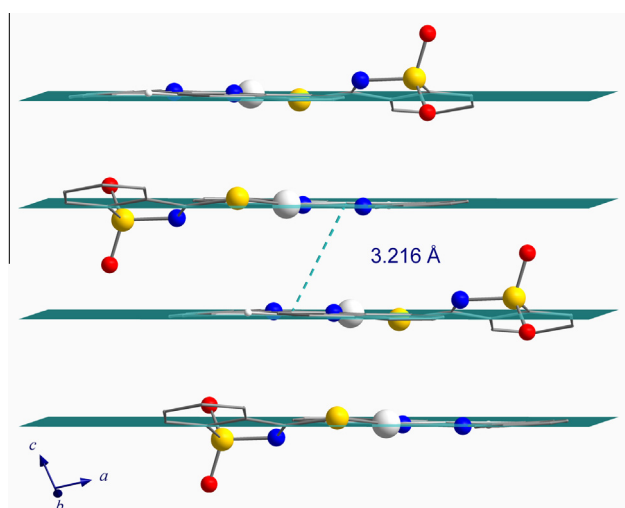|	Compound, nuclearity	pK_a[a]	Molar ratio[b]	Structure anion coordination	Ref.
8	*catena*-Poly-[Ag$_2$(tsac)$_2$(4-methylpyridine)]$_n$, polymeric	5.99	2:2:1	S, N-head to head	[12]
9	[Ag(collidine)$_2$)] [Ag(tsac)$_2$], Ionic complex salt	7.43	2:2:2	S-monocoordinated	[This work]

[a] Of the conjugate acid.
[b] Ag:tsac:ancillary ligand.

Fig. 7. Diagram of the layered structure of (**3**), with an interplanar distance of 3.216 Å. The dashed line connects the centroids of the facing 2,2′-biquinoline ligands.

sphere is constituted by the metal atom in a trigonal planar geometry made up from the S$_{exo}$ atoms of the thiosaccharinate ligand and the two N atoms of a 2,2′-biquinoline ligand, SAgN$_2$, with considerable deviation from the ideal angle of 120°, due to the small bite angle of the 2,2′-biquinoline ligand, 71.5(2)°. The remaining angles S1—Ag1—N11 and S1—Ag1—N21 are 134.25(16)° and 154.02(14)°, respectively. The four atoms are planar with a root mean square deviation of 0.0241 Å from their average plane. The short Ag–S$_{exo}$ distance (2.393(2) Å), together with the long C1–S$_{exo}$ bond distance (1.709(7) Å) reflects a S$_{exo}$ strongly coordinated to the metal center. The close interplanar distance, 3.216 Å, suggests the existence of a π–π interaction (Fig. 4) between pairs of 2,2′-biquin moieties. The powder X-ray diffraction pattern of the as prepared complex is very similar to the diffractogram simulated from the single crystal X-ray structure (Fig. S3 in Supplementary information).

3.3. Bonding modes of the thiosaccharinate ligand

In the last two structures presented here, of (**2**) and (**3·CH₃CN**), the thiosaccharinate ligand shows very different bonding modes.

We gather these structures together with structures resolved in our group in Table 5 for a comparison of the different binding modes seen in complexes with different pyridine based ancillary ligands, together with the pK_a of the pyridine based ligands. Considering silver thiosaccharinate complexes with the ancillary chelating N-donor ligands, in both the 2,2′-bipyridine (2,2′-bipy) complex, [Ag$_2$(tsac)$_2$(2,2′-bipy)$_2$] [8], and the 1,10′-phenanthroline (phen) complex, [Ag(tsac)(phen)]$_n$ [9], the thiosaccharinate anion bridges the silver atoms in a μ$_2$-S mode, lines 2 and 5. For the first, a centrosymmetric dinuclear complex is formed while for the second, an extended one dimensional structure is formed. In thiosaccharinate silver complexes with monodentate N-donor ligands, for example, in [Ag$_2$(tsac)$_2$py], py = pyridine, the thiosaccharinate ligand binds in a "*head-to-head*" μ$_2$-S,N coordination mode [10] (line 6) and in [Ag$_2$(tsac)$_2$(quin)$_2$] (line 3) the ligand binds in a "*head-to-tail*" arrangement [11]. In the one dimensional extended structures for *catena*-poly-[Ag(tsac)(3-methylpyridine)$_2$]$_n$ (line 7) and *catena*-poly-[Ag$_2$(tsac)$_2$(4-methylpyridine)]$_n$ (line 8) [12], the thiosaccharinate ligand binds just in μ$_2$-S fashion in the first and in a "*head-to-head*" μ$_2$-S,N in the second. The thiosaccharinate ligand always binds via the S$_{exo}$ atom to either just silver atom, or bridging between two in a μ$_2$-S mode to form dimeric or larger molecular complexes or to form one-dimensional extended structures. If the silver atom has a coordination site available, the N atom will also bind and the thiosaccharinate ligand chelates. The double complex salt [Ag(collidine)$_2$)][Ag(tsac)$_2$] (**2**) is the only ionic complex silver thiosaccharinate published to date. It is worth noting that the final structure of the complexes shows no correlation to the pK_a of the pyridine based ancillary ligands (Figs. 7 and 8).

3.4. ¹H and ¹³C nuclear magnetic resonance spectral studies of (**2**) and (**3**)

The ¹H and ¹³C NMR spectra of the new complexes, [Ag(2,4,6-coll)$_2$][Ag(tsac)$_2$] (**2**) and [Ag(tsac)(2,2′-bquin)]·CH₃CN (**3**), were recorded in DMSO-d_6 solutions. The numbering schemes of the complexes are shown in Scheme 3.

The ¹H NMR spectra of [Ag(2,4,6-coll)$_2$][Ag(tsac)$_2$] complex (**2**) presents the expected signals of the thiosaccharinate-protons as multiplets at 7.99–8.08 (H3), 7.86–7.95 (H6) and 7.75–7.83 (H4 & H5) ppm and the signals of the collidine ligand appear as three singlets at 6.96 (H10), 2.44 (H9) and 2.25 (H12) ppm. The last ones correspond to the methyl substituents. The ¹³C NMR spectrum shows the expected chemical shifts of the thioamidic C1 atom
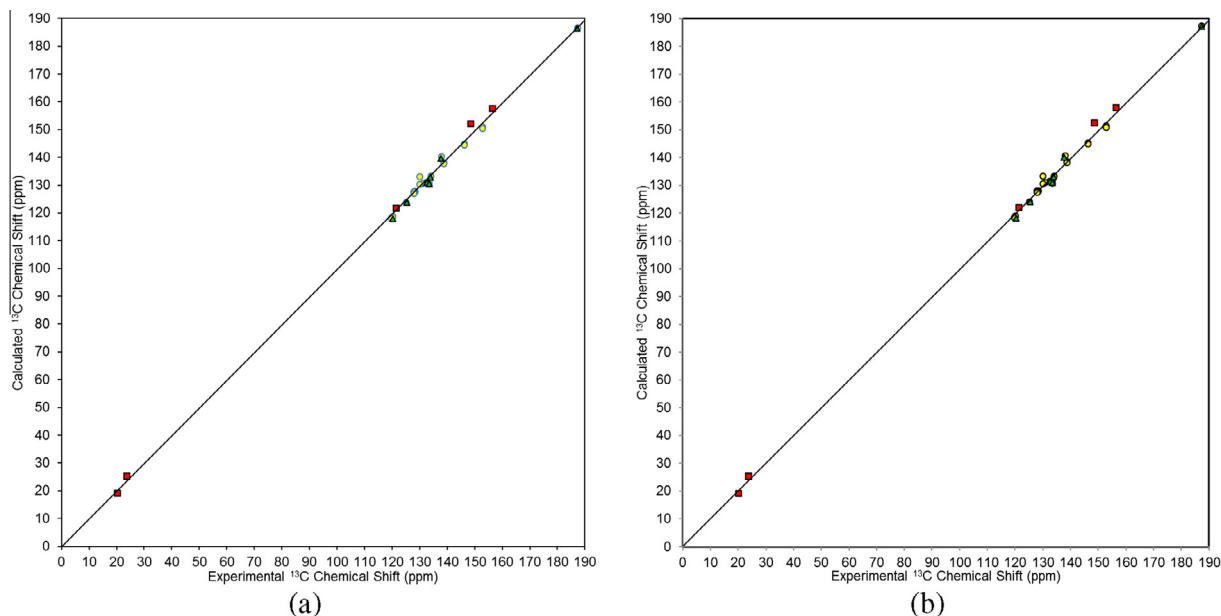
Fig. 8. Plot of calculated ^{13}C chemical shift experimental using the OLYP density functional (a) and HCTH93 density function (b) against experimental ^{13}C chemical shift for (**2**) and (**3**). The red squares are the cationic species of (**2**), the green triangles are the anionic part of (**2**) and the yellow circles are (**3**). (For interpretation of the references to color in this figure legend, the reader is referred to the web version of this article.)
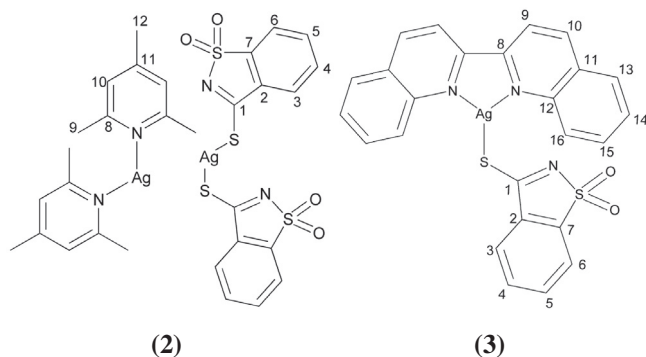
Scheme 3. Numbering scheme for complexes (**2**) and (**3**).

(located at 187.35 ppm) and those of the other six C atoms of the anions are in accordance with a monocoordinated thiosaccharinate, and agree with strongly coordinated anions. The carbon-signals of the collidine ligand are in accord with the structure of the complex (**2**).

The ^{1}H NMR spectra of [Ag(tsac)(2,2′-bquin)]·CH$_3$CN complex (**3**) shows three multiplets corresponding to the thiosaccharinate-proton signals at 8.04–8.08 (H3), 7.85–7.95 (H6) and 7.77–7.82 (H4 and H5) ppm. The aromatic protons of the biquinoline moiety appears at 8.72–8.81 ppm as a doublet of doublets corresponding to H9 and H10, two doublets at 8.51 (H16) and 8.13 (H13) ppm and two triplets, one at 7.74 (H14) ppm and another partially super-imposed with a thiosaccharinate multiplet (7.85–7.95 ppm) corresponding to H15. The ^{13}C NMR spectrum shows the expected signals of the thiosaccharinate and the aromatic *N*-donor ligand. The characteristic signal of the thioamidic C1 atom is located at 187.43 ppm, and is in agreement with the expected position for a mono-coordinated thiosaccharinate via the S$_{exo}$ atom [8].

3.5. Vibrational spectra

The spectra in the infrared (IR) region of the three complexes were recorded as KBr dispersions. The vibrational spectra of the three complexes are consistent with the X-ray and NMR structures. The most relevant bands are the ones related to the vibrations of the five membered rings of the anions, as they are displaced upon coordination to the nuclei located between 1500 and 400 cm^{-1}. The bands attributable to the N–H bond vibrations, namely v (NH) and δ(NH), which in the free ligand appears at 3341 and 1376 cm^{-1}, respectively, are absent in the spectra of both complexes. Since there are also no bands between 3000 and 2550 cm^{-1} (the v(SH) absorption region) we concluded that the ligand is in the deprotonated form in both complexes, as corroborated by the X-ray and NMR analysis. The similarities showed by the IR spectra of complexes **2** and **3** suggest that the anions may coordinate in the same monodentated fashion through the exo-cyclic sulfur atom. The coordination of the anions in [Ag(tsac) (2,2′-bquin)]·CH$_3$CN and [Ag(2,4,6-coll)$_2$][Ag(tsac)$_2$] complexes is reflected in the position of the band principally due to the stretching of the C–S$_{exo}$ bond (located at 1000 and 999 cm^{-1}, respectively), red shifted if it is compared to the free thiosaccharinate in PNP(tsac) (1010 cm^{-1}) [63]. In addition, the presence of the ligand molecules is confirmed by comparison with the results of Ozel et al. that studied the influence of the formation of bidentate coordination through both ring's nitrogen atoms on the vibrational wavenumbers of biquinoline [9,64].

3.6. Theoretical calculations

In order to understand the structure of complex (**2**), unique for a silver thiosacharinate, from a theoretical point of view, quantum chemical investigations have been carried out using the DFT formalism. The gas phase geometric structures of complexes (**2**) and (**3**) were optimized and the vibrational spectra were predicted. The results obtained are a good reproduction of the experimentally observed structural parameters (see Tables 3 and 4). The differences between the experimental and theoretical results can be attributed to the crystal packing forces. The nature of the vibration modes corresponding to complexes (**2**) and (**3**) were in agreement with the calculated. The experimental and calculated wavenumbers for some selected normal vibration modes are shown in

Table 6
Selected observed and calculated wavenumbers (cm^{-1}) of the anions for complexes (**2**) and (**3**).

	[Ag(2,4,6-coll)$_2$][Ag(tsac)$_2$] (**2**)		[Ag(tsac)(2,2'-bquin)] (**3**)	
	Experimental	Calculated (DFT)	Experimental	Calculated (DFT)
ν(NC),ν(CS), δ_{PhH},ν (CC)	1422w	1459	1410m	1474
ν_{as}(SO$_2$)	1310s	1336	1309s	1319
ν_{as}(ϕCN),δ(CH)	1234s	1246	1227m	1247
ν_s(SO$_2$),ν(CC)	1164vs	1137	1163s	1162
ν_s(SO$_2$),δ(ϕSN)	1124w	1160	1121w	1137
ν(CS),δ(CNS)	999m	1001	999m	1011
ν(NS),δ(CCC)	792m	781	807w	782

ν: stretching, δ: in plane bending, ϕ: benzene ring, as: asymmetric, s: symmetric. vs: very strong, s: strong, m: medium, w: weak.

Table 7
Performance of DFT functionals for theoretical ^{13}C magnetic constants for (**2**) and (**3**).

	DFT functional/NMR method			
	B3LYP/ GIAO	OLYP/ CSGT	OPBE/ CSGT	HCTH93/ CSGT
Best fit δ_{ref} (ppm)	177.2440	177.9255	181.6682	177.6273
Mean absolute deviation	9.2995	1.4900	2.3828	1.3468
RMS deviation	2.1673	1.4005	2.0312	1.2836
Maximum error	18.0966	3.2756	5.0827	3.6701
Slope	1.0798	0.9980	0.9840	0.9980
R^2	0.9980	0.9988	0.9991	0.9984

Table 6. The free energies calculations confirm the exothermicity of the formation of complex (**2**), 2.91 eV, obtained as the difference between the total energy of the optimized complex [Ag(coll)$_2$][Ag (tsac)$_2$] and the sum of the total energies of the optimized [Ag(coll)$_2$]$^+$ cation and [Ag(tsac)$_2$]$^-$ anion.

The solution phase NMR isotropic magnetic shielding for **2** and **3** in DMSO solvent was also studied with DFT calculations. Considering that the calculated NMR is extremely dependent on the geometry used, the geometries of the individual species, in DMSO solvent using the integral equation formalism model (IEFPCM) in GAUSSIAN 09 with the built in parameters for this solvent, were optimized using B3LYP hybrid DFT functional with the LanL2DZ ECP basis set for Ag and 6-31(2d,p) basis sets for the other elements. Global minimums were confirmed with vibrational frequency analyses of the optimized structures. The NMR solution phase chemical shifts for (**2**) and (**3**) were determined using the hybrid functionals B3LYP—very widely studied and known to produce reasonable, but not great, results [65,66]—, B97-2 and B98 with the GIAO method and the newer generalized gradient GGA DFT functionals HCTH93, OPBE and OLYP with the CSGT method, all with the DZP complete core basis set for Ag, EPR-III basis sets for H, C, N and O and aug-cc-pvdz for S. Both GIAO and CSGT methods produce similar results when large basis sets are employed [67]. The DFT functionals B97-2 and B98 did not achieve adequate convergence of the self-consistent field for some species and are not considered furthermore. For comparison, the magnetic shieldings were converted to chemical shifts ($\delta = \sigma_{ref} - \sigma$) using best fit σ_{ref} values for each DFT functional. The results are summarized in Table 7. B3LYP did not as perform well as the newer density funcionals. The OPBE functional, despite being labeled as promising [68], did not perform as well as the OLYP and HCTH93 functionals which performed equally well. The relative magnetic shielding for these last two showed an extremely small systematic error, both with $\sigma_{experimental} = 0.9980\sigma_{calculated}$. The mean absolute deviations are

similar with HCTH93 slightly better, as are the largest absolute deviations with OLYP slightly better for this. The chemical shifts, relative to TMS calculated in the same way as the Ag species, show consistent large errors.

4. Conclusions

In this paper, the synthesis of three silver thiosaccharinate complexes, [Ag$_2$(tsac)$_2$]·DMF (**1·DMF**), [Ag(2,4,6-coll)$_2$][Ag(tsac)$_2$] (**2**) and [Ag(tsac)(bquin)]·CH$_3$CN (**3·CH$_3$CN**) with their characterization by IR and ^{1}H and ^{13}C NMR spectroscopic methods as well as their single crystal X-ray structures are presented. The geometric parameters and IR spectra were confirmed by electronic gas phase calculations. The ^{13}C NMR data were compared with solvated phase electronic calculations; the OLYP and HCTH93 DFT functionals with the CSGT method both gave results that correlated well with the experimental values. The resulting structures showed great diversity: dinuclear for (**1**), ionic for (**2**) and mononuclear complex for (**3**); and in the first, the thiosaccharinate ligand bridges two silver cations, while in the other two it is monocoordinated. A comparison of the bonding modes of the thiosaccharinate ligand in known silver thiosaccharinate complexes with N-donor co-ligands was made, however, it was not possible to relate the differences among the properties of the N-donor co-ligands with the differences in the structures.

Author contributions

The manuscript was written through contributions of all authors. All authors have given approval to the final version of the manuscript.

Appendix A. Supplementary material

CCDC 1437754, 1437755 and 1437756 contains the supplementary crystallographic data for [Ag$_2$(tsac)$_2$]·DMF (**1**), [Ag(2,4,6-coll)$_2$] [Ag(tsac)$_2$] (**2**) and [Ag(tsac)(bquin)]·CH$_3$CN (**3**), respectively. These data can be obtained free of charge from The Cambridge Crystallographic Data Centre via www.ccdc.cam.ac.uk/data_request/cif. Supplementary data associated with this article can be found, in the online version, at http://dx.doi.org/10.1016/j.ica.2016.05.004.

References

[1] M. Dennehy, G.P. Tellería, S.H. Tarulli, O.V. Quinzani, S.D. Mandolesi, J.A. Guida, G.A. Echeverría, O.E. Piro, E.E. Castellano, Inorg. Chim. Acta 360 (2007) 3169.
[2] S.H. Tarulli, O.V. Quinzani, O.E. Piro, E. Baran, E.E. Castellanos, Monatsh. Chem. 132 (2001) 779.

[3] S.H. Tarulli, O.V. Quinzani, E.J. Baran, O.E. Piro, Z. Anorg. Allg. Chem. 628 (2002) 751.
[4] S.H. Tarulli, O.V. Quinzani, O.E. Piro, E.E. Castellano, E.J. Baran, J. Mol. Struct. 797 (2006) 56.
[5] S.H. Tarulli, O.V. Quinzani, O.E. Piro, E.E. Castellano, E.J. Baran, Z. Anorg. Allg. Chem. 629 (2003) 1975.
[6] D.R. Pérez, S.H. Tarulli, O.V. Quinzani, J. Dristas, R. Faccio, L. Suescun, A.W. Mombrú, Z. Anorg. Allg. Chem. 633 (2007) 1066.
[7] M. Dennehy, O.V. Quinzani, R.A. Burrow, Acta Crystallogr., Sect. C 63 (2007) m395.
[8] M. Dennehy, O.V. Quinzani, M. Jennings, J. Mol. Struct. 841 (2007) 110.
[9] M. Dennehy, S.D. Mandolesi, O.V. Quinzani, M. Jennings, Z. Anorg. Allg. Chem. 633 (2007) 2746.
[10] M. Dennehy, O.V. Quinzani, R.M. Ferullo, S.D. Mandolesi, N. Castellani, M. Jennings, Polyhedron 27 (2008) 2243.
[11] M. Dennehy, O.V. Quinzani, A. Granados, R.A. Burrow, Polyhedron 29 (2010) 1344.
[12] M. Dennehy, E. Freire, R. Baggio, Acta Crystallogr. C86 (2012) m17.
[13] M. Dennehy, G.P. Tellería, O.V. Quinzani, G.A. Echeverría, O.E. Piro, E.E. Castellano, Inorg. Chim. Acta 362 (2009) 2900.
[14] M. Dennehy, O.V. Quinzani, S.D. Mandolesi, R.A. Burrow, J. Mol. Struct. 998 (2011) 119.
[15] M. Dennehy, O.V. Quinzani, R. Faccio, E. Freire, Á.W. Mombrú, Acta Crystallogr., Sect. C 68 (2012) m12.
[16] M. Vieites, D. Gambino, M. Gonzalez, H. Cerecetto, J. Coord. Chem. 59 (2006) 101.
[17] M. Dennehy, O.V. Quinzani, A. Granados, R.A. Burrow, Inorg. Chim. Acta 377 (2011) 77.
[18] P.C. Andrews, R.L. Ferrero, C.M. Forsyth, P.C. Junk, J.G. Maclellan, R.M. Peiris, Organometallics 30 (2011) 6283.
[19] M. Dennehy, R.M. Ferullo, E. Freire, R. Baggio, Acta Crystallogr., Sect. C 70 (2014) 627.
[20] S.A. Al-Jibori, M.H.S. Al-Jibori, G. Hogarth, Inorg. Chim. Acta 398 (2013) 117.
[21] S.A. Al-Jibori, A.T. Habeeb, G.H.H. Al-Jibori, N.A. Dayaaf, K. Merzweiler, C. Wagner, H. Schmidt, G. Hogarth, Polyhedron 67 (2014) 338.
[22] S.A. Al-Jibori, Q.K.A. Al-Jibori, H. Schmidt, K. Merzweiler, C. Wagner, G. Hogarth, Inorg. Chim. Acta 402 (2013) 69.
[23] K. Nomiya, K. Tsuda, T. Sudoh, M. Oda, J. Inorg. Biochem. 68 (1997) 39.
[24] K. Nomiya, S. Takahashi, R. Noguchi, J. Chem. Soc., Dalton Trans. (2000) 2091.
[25] E.S. Raper, Coord. Chem. Rev. 165 (1997) 475.
[26] S. Schibye, R.S. Pedersen, S.O. Lawesson, Bull. Soc. Chim. Belg. 87 (1978) 229.
[27] R.G. Parr, W. Yang, Density Functional Theory of Atoms, Molecules, Oxford University Press, New York, 1988.
[28] A.D. Becke, J. Chem. Phys. 98 (1993) 5648.
[29] C. Lee, W. Yang, R.G. Parr, Phys. Rev. B 37 (1988) 785.
[30] S.H. Vosko, L. Wilk, M. Nusair, Can. J. Phys. 58 (1980) 1200.
[31] P.J. Stephens, F.J. Devlin, C.F. Chabalowski, M.J. Frisch, J. Phys. Chem. 98 (1994) 11623.
[32] M.J. Frisch, G.W. Trucks, H.B. Schlegel, G.E. Scuseria, M.A. Robb, J.R. Cheeseman, G. Scalmani, V. Barone, B. Mennucci, G.A. Petersson, H. Nakatsuji, M. Caricato, X. Li, H.P. Hratchian, A.F. Izmaylov, J. Bloino, G. Zheng, J.L. Sonnenberg, M. Hada, M. Ehara, K. Toyota, R. Fukuda, J. Hasegawa, M. Ishida, T. Nakajima, Y. Honda, O. Kitao, H. Nakai, T. Vreven, J.A. Montgomery Jr., J.E. Peralta, F. Ogliaro, M. Bearpark, J.J. Heyd, E. Brothers, K.N. Kudin, V.N. Staroverov, T. Keith, R. Kobayashi, J. Normand, K. Raghavachari, A. Rendell, J.C. Burant, S.S. Iyengar, J. Tomasi, M. Cossi, N. Rega, J.M. Millam, M. Klene, J.E. Knox, J.B. Cross, V. Bakken, C. Adamo, J. Jaramillo, R. Gomperts, R.E. Stratmann, O. Yazyev, A.J. Austin, R. Cammi, C. Pomelli, J.W. Ochterski, R.L. Martin, K. Morokuma, V.G. Zakrzewski, G.A. Voth, P. Salvador, J.J. Dannenberg, S. Dapprich, A.D. Daniels, O. Farkas, J.B. Foresman, J.V. Ortiz, J. Cioslowski, D.J. Fox, Gaussian 09, Revision C.01, Gaussian, Inc, Wallingford CT, 2010.
[33] G. Scalmani, M.J. Frisch, J. Chem. Phys. 132 (2010) 114110.
[34] P.J. Wilson, T.J. Bradley, D.J. Tozer, J. Chem. Phys. 115 (2001) 9233.
[35] A.D. Becke, J. Chem. Phys. 109 (1998) 2092.
[36] R. Ditchfield, Mol. Phys. 27 (1974) 789.
[37] F.A. Hamprecht, A.J. Cohen, D.J. Tozer, N.C. Handy, J. Chem. Phys. 109 (1998) 6264.
[38] N.C. Handy, A.J. Cohen, Mol. Phys. 99 (2001) 403.
[39] W.-M. Hoe, A. Cohen, N.C. Handy, Chem. Phys. Lett. 341 (2001) 319.
[40] T.A. Keith, R.F.W. Bader, Chem. Phys. Lett. 210 (1993) 223.
[41] C.L. Barros, P.J.P. de Oliveira, F.E. Jorge, Mol. Phys. 108 (2010) 1965.
[42] D. Feller, J. Comput. Chem. 17 (1996) 1571.
[43] K.L. Schuchardt, B.T. Didier, T. Elsethagen, L. Sun, V. Gurumoorthi, J. Chase, J. Li, T.L. Windus, J. Chem. Inf. Model. 47 (2007) 1045.
[44] APEX2 (v. 2014.9-0), BIS (v. 2.0.1.9), COSMO (v. 1.56), SAINT (v. 8.34a), SADABS (v. 2014/4), Bruker AXS Inc., Madison, Wisconsin, USA, 2014.
[45] SHELXTL (v.2014/4), Bruker AXS Inc., Madison, Wisconsin, USA, 2014.
[46] K. Brandenburg, H. Putz, DIAMOND Crystal, Molecular Structure Visualization (Version 3.1k), Crystal Impact, Bonn, Germany, 2014.
[47] C.F. Macrae, I.J. Bruno, J.A. Chisholm, P.R. Edgington, P. McCabe, E. Pidcock, L. Rodriguez-Monge, R. Taylor, J. van de Streek, P.A. Wood, J. Appl. Crystallogr. 41 (2008) 466.
[48] A.L. Spek, J. Appl. Crystallogr. 36 (2003) 7.
[49] G.A. Bowmaker, Inorg. Chim. Acta 358 (2005) 4307.
[50] C.Y. Chen, J.Y. Zeng, H.M. Lee, Inorg. Chim. Acta 360 (2007) 21.
[51] M. Thommes, K. Kaneko, A.V. Neimark, J.P. Olivier, F. Rodriguez-Reinoso, J. Rouquerol, K.S.W. Sing, Pure Appl. Chem. 87 (2015) 1051.
[52] J.C. Groen, L.A.A. Peffer, J. Pérez-Ramírez, Micropor. Mesopor. Mater. 60 (2003) 1.
[53] B.C. Lippens, J.H. de Boer, J. Catal. 4 (1965) 319.
[54] O. Kristiansson, Inorg. Chem. 40 (2001) 5058.
[55] H. Schmidbaur, A. Schier, Angew. Chem., Int. Ed. 54 (2015) 746.
[56] C.H. Suresh, N. Koga, J. Phys. Chem. A 105 (2001) 5940.
[57] A. van der Bondi, J. Phys. Chem. 68 (1964) 441.
[58] G.A. Bowmaker, Inorg. Chim. Acta 358 (2005) 4342.
[59] A.D. Bond, J. Davies, Acta Crystallogr. E57 (2001) o1141.
[60] S. Akyüz, T. Akyüz, J.E.D. Davies, Vib. Spectrosc. 22 (2002) 11.
[61] S.A. Moya, J. Guerrero, R. Pastene, I.A. Guzman, A.J. Pardey, Polyhedron 21 (2002) 439.
[62] A. Bishop, M.A. Turner, L.B. Kool, J. Organomet. Chem. 553 (1998) 53.
[63] M. Dennehy, O.V. Quinzani, S.D. Mandolesi, J.A. Güida, G.A. Echeverría, O.E. Piro, Monatsh. Chem. 138 (2007) 669.
[64] A.E. Ozel, S. Kecel, Vib. Spectrosc. 48 (2008) 238.
[65] M. Bühl, M. Kaupp, O.L. Malkina, V.G. Malkin, J. Comput. Chem. 20 (1999) 91.
[66] J.C. Facelli, Prog. Nucl. Magn. Reson. Spectrosc. 58 (2011) 176.
[67] J.R. Cheeseman, G.W. Trucks, T.A. Keith, M.J. Frisch, J. Chem. Phys. 104 (1996) 5497.
[68] Y. Zhang, A. Wu, X. Xu, Y. Yan, Chem. Phys. Lett. 421 (2006) 383.